Proceedings of the ASME 2020
Conference on Smart Materials, Adaptive Structures and Intelligent Systems
SMASIS2020
September 14-16, 2020 Irvine, CA, USA

SMASIS2020-2436

DESIGN AND OPTIMIZATION OF PIEZOELECTRIC ACTUATORS FOR AEROACOUTIC NOISES CONTROL IN A TURBOFAN

M. Perez[1], M. Ezzine[1,2], K. Billon[1], V. Clair[2], J. Marjono[3], and M. Collet[1]

[1] Université de Lyon, Ecole Centrale de Lyon, ENISE, ENTPE, CNRS, Laboratoire de Tribologie et Dynamique des Systèmes LTDS UMR5513, F-69134, Ecully, France
[2] Université de Lyon, Ecole Centrale de Lyon, INSA Lyon, Université Claude Bernard Lyon 1, CNRS, Laboratoire de Mécanique des Fluides et d'Acoustique LMFA UMR5509, F-69134, Ecully, France
[3] Safran Aircraft Engines, F-77550, Moissy-Cramayel, France

ABSTRACT

This paper reports on the design and optimization of different types of piezoelectric actuators for aeroacoustic control applications. This study was carried out within the context of the European project CleanSky2/InnoSTAT. The aim of our work is to reduce the aeroacoustic noises that appear in an airplane turbofan by adding an area of piezoelectric actuators on the Outlet Guide Vanes. These piezoelectric structures will subsequently be controlled with an active approach and tested in the open-jet anechoic wind tunnel at LMFA. The noise source which has to be reduce/control comes from vortices located in the turbulent flow (which can for example be created by the fan module) interacting with the stator blades. The predominant frequencies and the pressure fluctuations levels related to these vortices rely on the airflow speed and are fixed between 1000Hz and 2000Hz in our case. To reach the target, we plan to manufacture an area of piezoelectric actuators on the intrados and the extrados of the stator blades in order to control the response of the blades to the turbulence of the airflow responsible for the aeroacoustic noise. Several adjacent blades will be equipped with this type of transducers. This study outline the design and the optimization of each piezoelectric cell in order to achieve good results in the frequency range previously defined as well as an acceptable mechanical strength of the blade. A most detailed study on the active shunt will be investigate later on.

Keywords: Turbofan, aeroacoutic noises, piezoelectric actuators, active control

1. INTRODUCTION

Aircraft turbofan engines are noisy during take-off, flyover and landing operations. The noise generated is primarily due to intake and rearward radiation from the fan stage. Passive technologies, such as liners, are already applied for noise reduction in commercialized aircraft but future engines will require additional noise reductions to satisfy ever more stringent regulations. There are many possibilities for further improvement and one of them is to work on the design of the OGV (also called stator) located downstream of the fan in the bypass duct. The EU-funded InnoSTAT project aims to bring several OGV concepts (figure 1) to TRL 3 on full scale.

Since 2000, a lot of work has been dedicated to piezoelectric devices integrated into aeronautic structures. So far, they were aiming at increasing the aerodynamic performances rather than to reducing the aeroacoustic noise. For example, piezoelectric devices have been investigated: (i) at the trailing edge of helicopters and aircraft blades [1-3], (ii) at the leading edge of a

blade [4], (iii) spread across the pressure and suction side of a blade [5-6] and even positioned inside the nacelle [7].

What is being proposed here is to integrate an array of piezoelectric actuators on the stator vanes which will be coupled to an active control strategy [8]. This paper will be focused on the optimization of the efficiency of the piezoelectric cells.

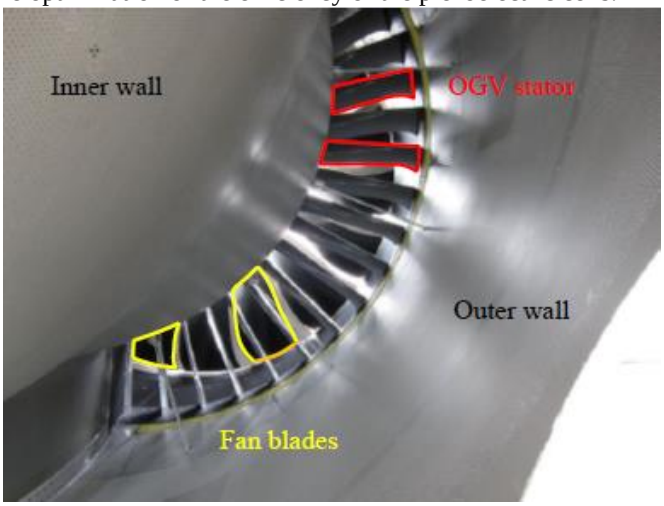

FIGURE 1: PICTURE TAKEN FROM THE BYPASS DUCT OF A REDUCED SCALE TURBOFAN IN THE EQUIPEX PHARE-2 TEST RIG

2. OPTIMIZATION OF THE PIEZOELECTRIC CELLS

This section will be devoted to the optimization of three architectures of piezoelectric actuators. In this specific context, the purpose is to design "efficient" cells able to work in the targeted frequency range. First calculations and measurements allowed to identify that the spectrum of the pressure fluctuations responsible for the aeroacoustic noise generated around the stator is highly energetic between 1000 and 2000Hz. At this stage, it is necessary to introduce f_{OCi} the i^{th} resonance frequency of the cell when the piezoelectric element is open circuited and f_{SCi} the i^{th} short circuit resonance frequency. Thus, the mean resonance frequency of the i^{th} mode can be define as:

$$f_{mean\_i} = \frac{f_{oci}+f_{sci}}{2} \quad (1)$$

As well as the modal electromechanical effective coupling coefficient:

$$k_{effi}{}^2 = \frac{f_{oci}{}^2+f_{sci}{}^2}{f_{sci}{}^2} \quad (2)$$

Hence, the optimization suggested here is to maximize the modal electromechanical effective coupling coefficient of the first mode $k_{eff1}{}^2$ [8-9] while maintaining the mean resonance frequency of the first mode to f_{mean_1}=1500Hz. In this study, structural steel skins, PZT-5A piezoelectric structures and tungsten masses will be considered, with the properties detailed in Table 1. All the following results were obtained by FE computations.

TABLE 1: PROPERTIES OF THE DIFFERENT MATERIALS

Material		Structural Steel
Structural Steel	Density [kg.m^{-3}]	7850
	Young modulus [GPa]	300
	Poisson's ratio [1]	0.3
PZT-5A	Density [kg.m^{-3}]	7750
	Elastic coefficients [GPa]	C_{E11}==C_{E22}=120 C_{E33}=110 C_{E44}=C_{E55}=C_{E66}=21 C_{E12}=C_{E13}=C_{E23}=C_{E21}=C_{E31}=C_{E32}=75
	Piezoelectric coefficients [C.N^{-1}]	d_{31}=d_{32}=-1.71×10^{-10} d_{33}=3.74×10^{-10} d_{24}=d_{15}=5.84×10^{-10}
Tungsten	Density [kg.m^{-3}]	17800
	Young modulus [GPa]	360
	Poisson's ratio [1]	0.28

2.1 Concept 1

This first concept consists in adding two piezoelectric patches under a thin layer with a consistent thickness. With vertically polarized piezoelectric patches and horizontal electrodes, as shown in Figure 2, the piezoelectric structures will be able to operate in d_{31} mode. L_c denotes the width of the cell, e_c the thickness of the skin, L_p the overall width of the piezoelectric patches, e_p the thickness of each piezoelectric patch, and $x_p/2$ the offset of each piezoelectric patch.

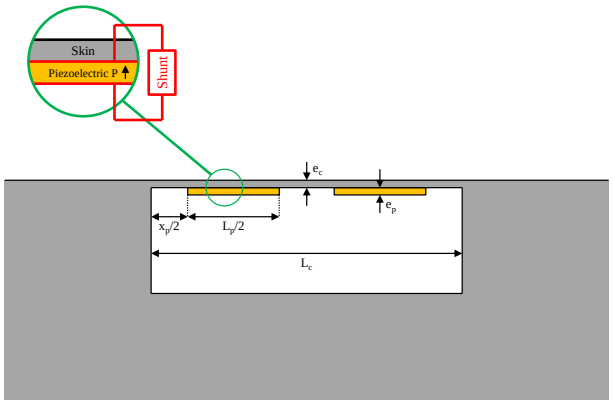

FIGURE 2: CONCEPT 1, CELL WITH A SIMPLE PIEZOELECTRIC PATCHES IN d_{31} OPERATION

Figure 3 highlights that doubling the number of piezoelectric patches is not relevant since the maximum effective coupling coefficient is achieved when the patches are come into contact i.e. x_p=L_c-L_p, thus forming an single centered piezoelectric patch.

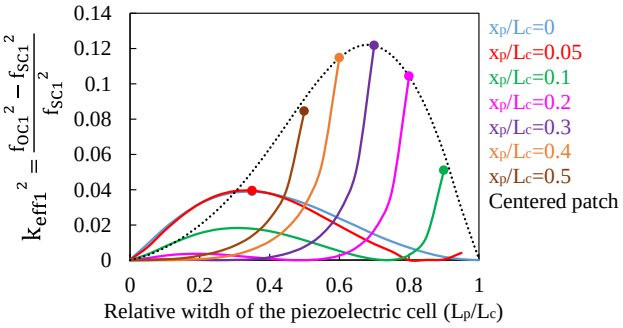

FIGURE 3: MODAL ELECTROMECHANICAL EFFECTIVE COUPLING COEFFICIENT DEPENDING TO L_p and x_p (concept 1, L_c=20mm, e_c=100µm, f_{mean_1}=1500Hz, e_{p_opt})

In this optimal configuration, Figure 4 shows the best results obtained with different skin thicknesses. It can be noted that a decrease of the thickness of the skin involves an increase of the size of the piezoelectric patch width and thickness as well as an increase of the modal electromechanical effective coupling coefficient. Indeed, if the skin is too stiff, it is easy to understand that a piezoelectric whose edges would be too close to the end of the skin will not be efficient. On the contrary, it is interesting to increase the width of the piezoelectric patch be with a more flexible skin. The increase of the thickness e_p allows to balance the loss of stiffness of the skin in order to keep f_{mean_1}=1500Hz. Finally, it is possible to achieve modal electromechanical effective coupling coefficients up to 0.16 (Figure 4).

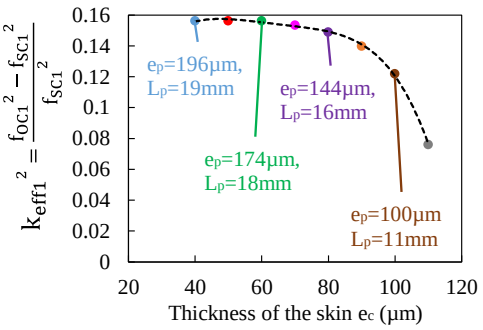

FIGURE 4: MODAL ELECTROMECHANICAL EFFECTIVE COUPLING COEFFICIENT ACCORDING TO THE THICKNESS OF THE SKIN (concept 1, L_c=20mm, centered patch: x_p=L_c-L_p, f_{mean_1}=1500Hz, e_{p_opt}, L_{p_opt})

2.2 Concept 2

The second concept is made up of several piezoelectric parts placed under a thin layer. As shown in Figure 5, the piezoelectric components are horizontally polarized and vertical electrodes are incorporated in order to operate in d_{33} mode. A tungsten central mass is also added to increase the thickness of the skin while maintaining a first mean resonance frequency close to 1500Hz. The cell will therefore be stiffer and more robust.

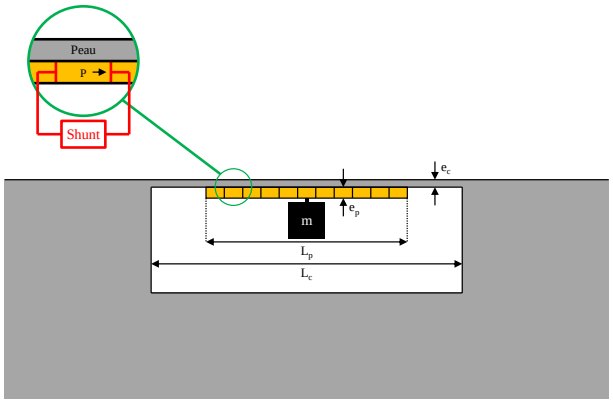

FIGURE 5: CONCEPT 2, CELL WITH A PIEZOELECTRIC STACK IN d_{33} OPERATION

First of all, it can be noticed that, without added mass, k_{eff1} tend towards 0.3 by reducing the thickness of the skin (blue curve in Figure 6). This demonstrates that this concept is two times more efficient than the previous one. Then, it can be stated that the influence of the tungsten mass is to slightly reduce the performances of the cell as a result of the non-zero width of the attachment point. However, it is then noticeable that an increase of the mass does no longer have any effect on the maximum value of k_{eff1}, provided that the thickness of the skin is small enough. For example, k_{eff1}=0.244 with e_c=200µm and m=284.8mg.mm^{-1} which is equivalent to k_{eff1}=0.252 with e_c=150µm and m=160.2mg.mm^{-1}, or k_{eff1}=0.258 with e_c=100µm and m=71.2mg.mm^{-1}. Therefore, the parameter m can provides a simple adjustment parameter to set the robustness of the cell.

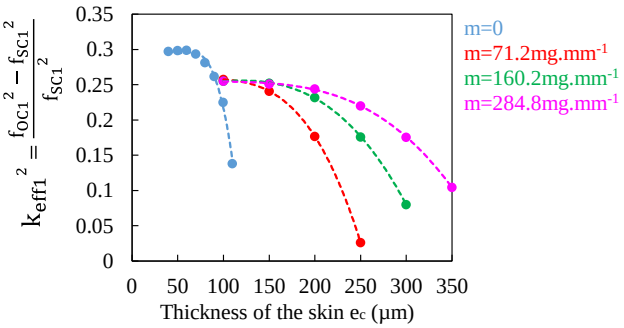

FIGURE 6: MODAL ELECTROMECHANICAL EFFECTIVE COUPLING COEFFICIENT (concept 2, L_c=20mm, f_{mean_1}=1500Hz, e_{p_opt}, L_{p_opt})

2.3 Concept 3

This final concept is very close to the previous one with isolated piezoelectric structures in d_{33} operation. This design is intended to be more realistic, with a larger cell width (L_c=4cm), in order to achieve even lower natural frequencies. Insulating spacers were also included (purple in Figure 7) to separate the piezoelectric structures and allow a simpler solution for electrical wiring. Air gaps are also added above each piezoelectric element to avoid any electrostatic issue. The width of the spacers is selected via the overall width of the piezoelectric

elements L_p, and the air gaps are entirely controlled by the parameter e_r (Figure 7).

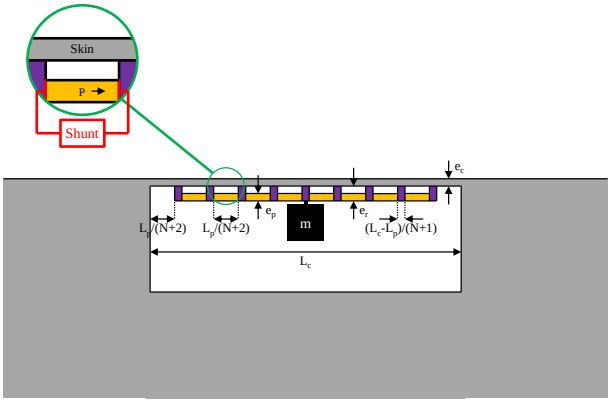

FIGURE 7: CONCEPT 3: FINAL DESIGN OF THE CELL WITH N=8 PIEZOELETRIC ELEMENTS

This final design allows to achieve a much lower dependency between the size of the piezoelectric structures and the first mean resonance frequency (Figure 8). It is thus possible to set e_c to obtain in the first instance a mean resonance frequency of the first mode around 1500Hz. We can then refine the optimization with the thickness e_p and the width L_p to fit more finely the mean resonance frequency of the first mode and maximize the modal electromechanical effective coupling coefficient (Figure 8 and Figure 9).

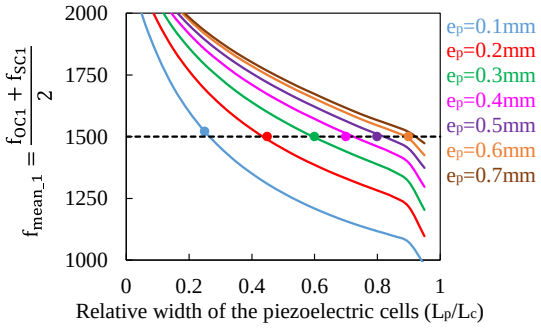

FIGURE 8: MEAN RESONANCE FREQUENCY OF THE FIRST MODE FOR DIFFERENT PIEZOELECTRIC DIMENSIONS (concept 3, L_c=40mm, e_c=0.6mm, e_r=1mm, m=445mg.mm^{-1})

Finally, the overall length of the piezoelectric structures L_p can be used to maximize the modal electromechanical effective coupling coefficient. In Figure 9, it can be observed that, on this example, the performances of these design are slightly smaller than the one obtained with the concept 2 (k_{eff12}=0.23 vs k_{eff12}=0.26). However, better results (higher than k_{eff12}=0.3) can be obtained by increasing e_r and decreasing e_p.

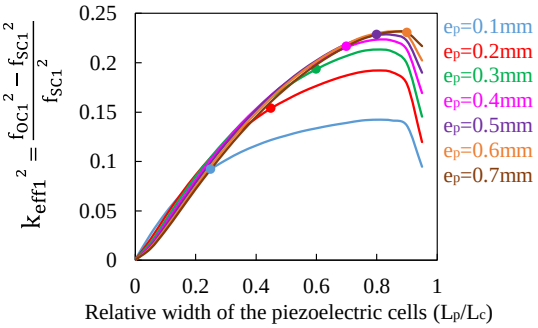

FIGURE 9: MODAL ELECTROMECHANICAL EFFECTIVE COUPLING COEFFICIENT FOR DIFFERENT PIEZOELECTRIC DIMENSIONS (L_c=40mm, e_c=0.6mm, e_r=1mm, m=445mg.mm^{-1})

3. CONCLUSION

In this paper, three designs of piezoelectric cells have been detailed and optimized to operate in the frequency range comprised between 1000 and 2000Hz. It appears from these computations that an operation in d_{33} mode is more efficient than an operation in d_{31} mode in this specific case. Adding weight is crucial in order to achieve "low frequency" cm-scale cells able to operate in a harsh aeronautical environment. These cells will subsequently be manufactured, assembled, coupled to a shunt active controller and laboratory-tested on a linear cascade of vanes in an open-jet anechoic wind tunnel.

ACKNOWLEDGEMENTS

The InnoSTAT project has received funding from the Clean Sky 2 Joint Undertaking (under grant agreement No 865007 The JU receives support from the European Union's Horizon 2020 research and innovation programme and the Clean Sky 2 JU members other than the Union. This publication reflects only the author's view and the JU is not responsible for any use that may be made of the information it contains.

REFERENCES

[1] Straub F.K. et al., Development of a piezoelectric actuator for trailing edge flap control of full scale rotor blades, *Smart materials and structures*, 2001

[2] Wickramasinghe T. et al., Numerical and experimental study of active flutter suppression with piezoelectric device for transonic cascade, *ASME turbo expo: Power for land, sea, and air*, 2008

[3] Pankonien A. et al., Experimental testing of spanwise morphing trailing edge concept, *Active and passive smart materials structures and integrated systems*, 2013

[4] Geisler W. at al., New rotor airfoil design procedure for unsteady flow control, *European rotorcraft forum*, 2000

[5] Remington P. et al., Active control of low-speed fan tonal noise using actuators mounted in stator vanes: Part 1 Control system design and implementation, *Aeroacoustic conference and exhibit*, 2003

[6] Duffy K.P. et al., Active piezoelectric vibration control of subscale composite fan blades, *Noise control engineering journal*, 2006

[7] Schulz J. et al., Active noise control in axial turbomachines by flow induced secondary sources, *Aeroacoustics conference and exhibit*, 2002

[8] Collet M. et al., Vibroacoustic diffusion optimization in beams and plates by means of distributed shunted piezoelectric patches, *Vibration and structural acoustics analysis*, 2011

[9] Livet S. et al., Structural multi-modal damping ratio by optimizing shunted piezoelectric transducers, *European journal of computational mechanics*, 2011